

Cite this: DOI: 10.1039/c0xx00000x

www.rsc.org/xxxxxx

ARTICLE TYPE

Energy level tuning of TPB-based hole-transporting materials for high efficient perovskite solar cells

Yakun Song,^{a,b} Songtao Lv,^c Xicheng Liu,^{a,b} Xianggao Li,^{a,b} Shirong Wang,^{a,b} Huiyun Wei,^c Dongmei Li,^c Yin Xiao^{a,b} and Qingbo Meng^{*c}⁵ Received (in XXX, XXX) XthXXXXXXXXXX 20XX, Accepted Xth XXXXXXXXXXXX 20XX

DOI: 10.1039/b000000x

Two TPB-based HTMs were synthesized and their energy levels were tuned to match with perovskite by introducing electron-donating groups asymmetrically. The TPBC based doping-free perovskite solar cell afforded an impressive PCE of 13.10% under AM 1.5G illumination, which is the first case for effective device with TPB-based doping-free HTMs.

Very recently, hybrid organic-inorganic perovskites ($\text{CH}_3\text{NH}_3\text{PbX}_3$, where X corresponds to halogenes) solar cells have attracted much attention due to their simple structure, low production cost and superb photovoltaic performance. Using 2,2',7,7'-tetrakis(N,N-di-p-methoxyphenylamine)-9,9'-spirobifluorene (spiro-OMeTAD) as a hole transporting material (HTM) to instead of liquid electrolytes in this hybrid solar cell, power conversion efficiencies (PCE) of over 15.0% were achieved under 1 sun (100 mW/cm^2).^{1,2,3,4} Although spiro-OMeTAD has been considered as the best candidate HTM for perovskite solar cells, intensive effort has been devoted to develop cheaper alternatives to spiro-OMeTAD. Several polymer hole conductors have been employed as HTM and the highest PCE was 12.0% based on PTAA.⁵ Compared to polymer HTMs, small-molecule HTMs benefit from the fact that they are easy to purify and easily form crystalline films for the fabrication of desired high efficiency devices. Various small-molecule HTMs, such as 3,4-ethylenedioxythiophene,⁶ pyrene,⁷ linear π -conjugated structure,⁸ butadiene,⁹ swivel-cruciform thiophene,¹⁰ oligothiophene,¹¹ tetrathiafulvalene,¹² quinolizinoacridine,¹³ and 1,3,5-triazine¹⁴ based HTMs have been developed and gave efficiency of 8.8–13.8%. Our group have reported the synthesis of several triphenylamine-based small-molecule HTMs, and impressive performances (PCE=11.6%) have been achieved with these HTMs.^{8,9} From the commercialization viewpoint, the exploration of efficient and cost-effective HTM is still the key challenge for further advancement of the hybrid perovskite solar cell.

N,N,N',N'-tetraphenyl-benzidine (TPB), as one essential HTM, has been widely used in diverse organic electronic devices such as organic light emitting diode (OLED), organic field-effect transistor (OFET), dye-sensitized solar cells (DSSC)^{15,16,17,18,19} etc. It also usually serve as building blocks for construction of largely conjugated HTM molecules due to its superb hole-transport ability.²⁰ Unfortunately, to the best of our knowledge, development and application of TPB-based HTM in perovskite

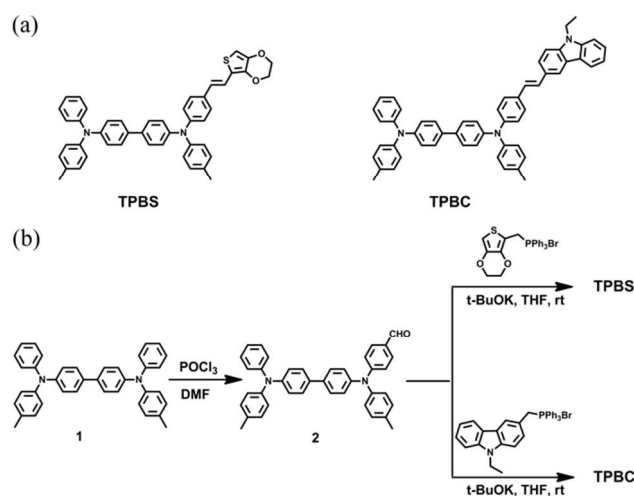


Fig. 1 (a) Molecular structures of HTMs; (b) Synthetic route for HTMs.

solar cell has been neglected. In our previous work, TPB was introduced into the perovskite solar cells to engineer the metal-semiconductor interface.²¹ The PCE increased by about 28 % after the interface modification. We also proved that TPB could enhance the interfacial resistance of $\text{CH}_3\text{NH}_3\text{PbI}_3/\text{Au}$ interface to favor the reduction of dark current effectively and lead to improvement in open-circuit voltage (V_{oc}). The higher LUMO of TPB compared to perovskite could block the electron transport and hence suppress the carrier recombination. However, the TPB exhibits deeper HOMO than that of perovskite, which is unfavorable to the hole transportation. The antagonistic contribution of electron-blocking and hole-transport lead to a relatively low PCE (6.71 %).²¹

Herein, we report the synthesis and characterization of two TPB-based HTMs (TPBS and TPBC) as shown in Fig.1 (a), as well as their application in perovskite solar cells. The device, fabricated with TPBC as HTM, achieves a PCE of 13.10% without doping under AM 1.5G (100 mW/cm^2) illumination. This results is comparable with that obtained using the well-known p-type doping spiro-OMeTAD. By simply introducing 3,4-ethylene-dioxythiophene (EDOT) and N-ethylcarbazol (NEC) to TPB skeleton, the energy levels of the TPB-core HTMs are tuned to match with the perovskite, which is expected to benefit hole transportation and retard electron transportation. Additionally, the nonplanar configuration of TPB core could be expected to

prevent close contact between the $\text{CH}_3\text{NH}_3\text{PbI}_3$ and HTMs, which favors to reduce electronic coupling and charge recombination.

The **TPB**-core HTMs were synthesized through a simple process with low cost based on Wittig reaction according to our previous report.²² The synthetic route for the HTMs is depicted in Fig. 1(b) and experimental details are given in the Electronic Supporting Information (ESI[†]). The new **TPB** derivatives (**TPBS** and **TPBC**) were fully characterized by ¹H NMR spectroscopy, high resolution mass spectrum, and elemental analysis (ESI[†]). All the analytical data are consistent with the proposed structures. The two HTMs have good solubility in commonly used solvents, such as dichloromethane, chloroform, tetrahydrofuran and toluene, etc.

The UV-vis absorption spectra of **TPBS**, **TPBC** and **TPB** in dichloromethane (DCM) are depicted in Fig. 2(a). As shown in the UV-vis spectra, the absorption band of **TPB** located in UV range. While for **TPBS** and **TPBC**, the extended conjugation length results in a red shift of their absorption band to visible range.²³ This suggests that by introduction of electron-donating moiety (EDOT and NEC) could increase the electron density in the **TPB** core and hence tunes the HOMO and the LUMO energy levels effectively. Besides, **TPBS** and **TPBC** exhibit fine structure (shoulder peak) in DCM due to the substitution on **TPB** core.

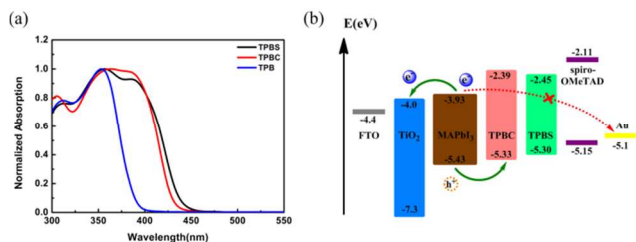


Fig. 2 (a) Normalized absorption spectra of **TPBS**, **TPBC** and **TPB** in DCM; (b) Energy level diagram of the corresponding materials used in perovskite solar cells.

The energy levels of these HTMs (Table 1) are determined using cyclic voltammetry (CV, Figure S1[†]) in dilute DCM solutions and relative data are listed in Table 1. It is found that both the HOMO levels of **TPBS** (-5.30 eV) and **TPBC** (-5.33 eV) are higher than that of **TPB** core (-5.52 eV), which is caused by the electron-donating effect of EDOT and NEC. Fig. 2 (b) shows the energy level diagram of the corresponding materials in the devices. The HOMO levels for **TPBS** and **TPBC** could well match with the valence band of $\text{CH}_3\text{NH}_3\text{PbI}_3$ (-5.43 eV), which is energetically favorable to the hole transfer at the interface. Furthermore, since the V_{oc} of solar cell is governed by the energy difference between the quasi-Fermi levels of the electrons in the TiO_2 and the HOMO of the HTM,⁶ **TPBS** and **TPBC** could be expected to afford a higher V_{oc} than spiro-OMeTAD for perovskite solar cell because of their deeper HOMO than spiro-OMeTAD (-5.15 eV). Besides, the LUMO levels of **TPBS** (-2.45 eV) and **TPBC** (-2.39 eV) are higher than the conduction band edge of $\text{CH}_3\text{NH}_3\text{PbI}_3$ (-3.93 eV), which could block the electron transportation from $\text{CH}_3\text{NH}_3\text{PbI}_3$ to Au and hence suppress the carrier recombination.²¹

Thermogravimetric analysis (TGA) and differential scanning calorimetry (DSC) measurements show that **TPBS** and **TPBC**

Table 1 Summary of the electrochemical, and thermal properties of **TPBS**, **TPBC**, **TPB** and **spiro-OMeTAD**

HTM	HOMO(eV)	LUMO(eV)	E_{gap} (eV)	T_g
TPBS	-5.30	-2.45	2.85	104
TPBC	-5.33	-2.39	2.94	105
TPB	-5.52	-2.27	3.25	77 ²⁰
spiro-OMeTAD	-5.15	-2.11	3.04	125 ¹⁰

have high decomposition temperatures (T_d , 381 °C and 474 °C for **TPBS** and **TPBC**, respectively) and glass transition temperatures (T_g , 104 °C and 105 °C for **TPBS** and **TPBC**, respectively) (Figure S2[†]). This result reveals that these two HTMs have excellent thermal stability to favor their practical application in device.

The hole transporting mobilities of **TPBS** and **TPBC** are evaluated by time-of-flight (TOF) measurements (Figure S3[†]). The hole mobility (μ) is calculated according to the equation $\mu = d^2/Vt_r$, where d , V and t_r is the film thickness, applied bias voltage and transit time, respectively. It is found that the hole-drift mobilities of **TPBS** and **TPBC** are 3.87×10^{-4} and $4.04 \times 10^{-4} \text{ cm}^2 \cdot \text{V}^{-1} \cdot \text{s}^{-1}$ respectively at an electric field of $2.3 \times 10^5 \text{ V} \cdot \text{cm}^{-1}$, which are little higher than that of **TPB** ($2.81 \times 10^{-4} \text{ cm}^2 \cdot \text{V}^{-1} \cdot \text{s}^{-1}$)¹⁸ and the well-known small molecular HTM spiro-OMeTAD ($2 \times 10^{-4} \text{ cm}^2 \cdot \text{V}^{-1} \cdot \text{s}^{-1}$ determined using the same technique²⁴). The high hole mobility indicated these HTMs could have great potential for application in perovskite solar cell.

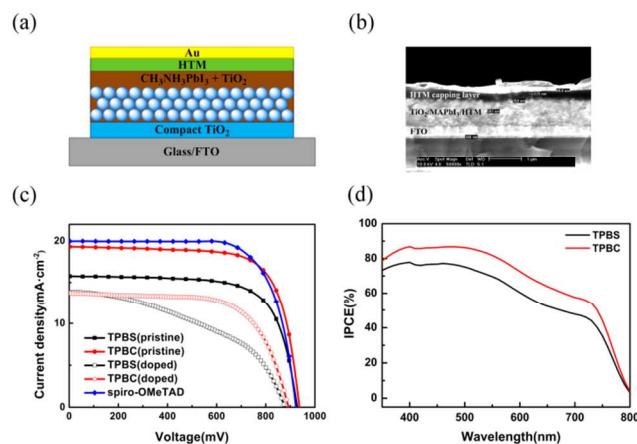


Fig. 3 (a) Diagrammatic representation of photovoltaic device structure; (b) Cross-sectional SEM image of the representative device; (c) $J-V$ curves for the perovskite solar cells fabricated with **TPBS**, **TPBC** and **spiro-OMeTAD**; (d) IPCE spectrum of the cell with **TPBS** and **TPBC**.

The photovoltaic performance of perovskite solar cells based on **TPBS** and **TPBC** as HTM without doping are evaluated. Device based on p-type doping spiro-OMeTAD as HTM is also fabricated for comparative study. Fig 3 (a) illustrates the structure of the perovskite solar cell. Clear interfaces in the device structure are observed in the cross-sectional scanning electron microscopy (SEM) image (Fig.3 (b)). The photocurrent density-voltage ($J-V$) curves for $\text{FTO}/\text{TiO}_2/\text{CH}_3\text{NH}_3\text{PbI}_3/\text{HTM}/\text{Au}$ solar cells are presented in Fig.3 (c) and related parameters are summarized in Table 2. As expected, the **TPBS** and **TPBC** give a higher V_{oc} than spiro-OMeTAD for device, which is commensurate with their deeper HOMO level. The best cell affords an open-circuit voltage (V_{oc}) of 942 mV, a short-circuit current density (J_{sc}) of 19.32 mA/cm^2 and a fill factor (FF) of

0.72, leading to a PCE of 13.10% under AM 1.5G ($100\text{ mW}\cdot\text{cm}^{-2}$) illumination. This result is comparable to that of spiro-OMeTAD with lithium bis(trifluoromethylsulfonyl)imide (LiTFSI) and 4-tert-butylpyridine (TBP) as dopant.¹³ However, devices based on p-doping **TPBS** and **TPBC** exhibit much poorer performance, especially in terms of *FF* and *J_{sc}*. Further investigation about the effect of dopant and optimization of doping process is in process. The IPCE spectrum of the cell with the two HTMs is presented in Fig. 3 (d). An integral photocurrent from the overlap of the IPCE spectrum is $15.2\text{ mA}\cdot\text{cm}^{-2}$ and $17.9\text{ mA}\cdot\text{cm}^{-2}$ for **TPBS** and **TPBC**, respectively, basically in agreement with the experimentally obtained *J_{sc}*.

Table 2 *J-V* characteristics of photovoltaic measurements ^a

HTM	<i>J_{sc}</i> /mA·cm ⁻²	<i>V_{oc}</i> /mV	<i>FF</i>	<i>η</i> / %
TPBS	15.75	932	0.70	10.29
TPBC	19.32	942	0.72	13.10
TPBS(doped)	13.83	879	0.45	5.48
TPBC(doped)	13.72	890	0.66	8.06
spiro-OMeTAD^b	20.03	921	0.72	13.28

^a Illumination: $100\text{ mW}\cdot\text{cm}^{-2}$ simulated AM 1.5 G solar light; the effective areas of devices are 0.08 cm^2 ; ^b doping with LiTFSI and TBP.

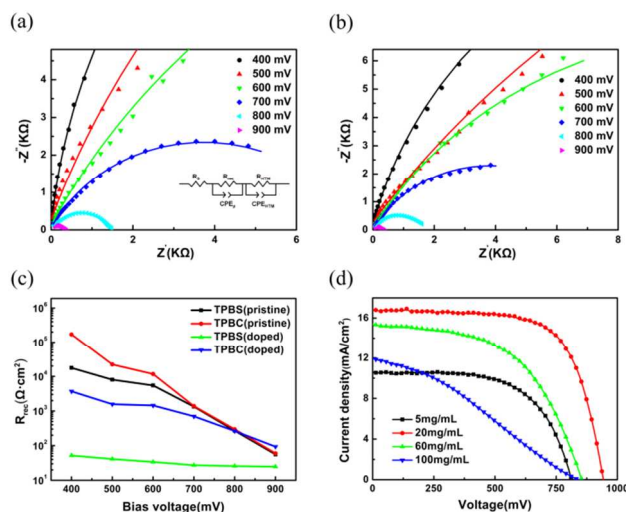


Fig.4(a) Nyquist plots of the device with thin layer **TPBS** in the dark over different forward biases, scattered point: experimental data, solid line: fitted curves; (b) Nyquist plots of the device with thin layer **TPBC** in the dark over different forward biases; (c) Plots of recombination resistance (*R_{rec}*) vs bias voltages for the devices with **TPBS** and **TPBC**; (d) *J-V* curves for the perovskite solar cells with different **TPBC** concentration.

The electrochemical impedance spectroscopy (EIS) analysis are carried out, in which the potential bias is applied from 400 to 900 mV in the dark in the frequency range from 10^5 to 0.1 Hz, as shown in Fig. 4 (a) and Fig. 4 (b). According to simplified transmission line model, the main arc mainly attribute to the combination of the recombination resistance (*R_{rec}*) and the chemical capacitance of the film (*CPE_μ*) (inset of Fig. 4(a)).^{25,26,27} By fitting the Nyquist plots, the bias voltage dependence of *R_{rec}* for both **TPBS** and **TPBC** is obtained (Fig.4(c)). For both HTMs, the declined *R_{rec}* are observed as the forward bias voltage increased, which could be ascribed the elevated Fermi level in the mesoscopic TiO₂ under the forward bias (>500mV).⁹ The larger *R_{rec}* of device with **TPBC** than **TPBS** at the same forward bias voltage suggests that **TPBC** as the HTM is superior to **TPBS** in

preventing charge recombination. The larger *R_{rec}* is supposed to favor improvement of photovoltaic performance, which is in agreement to the results listed in Table 2. As shown in Fig. 4(c), the decreased *R_{rec}* of device with p-doping **TPBS** and **TPBC** indicates more charge recombination and worse photovoltaic performance, which is in consistent with the results listed in Table 2. The Nyquist plots of the device based on p-type doped **TPBS** and **TPBC** in the dark over different forward biases are shown in Figure S4.

The **TPBC** is taken as a model HTM to further investigate the influence of HTM deposition amount on the cell performance. As shown in Fig 4 (d) and Table S1[†], the cell fabricated at very low HTM concentration (5 mg/mL) exhibits poor photovoltaic performance. This could be explained by the reason that effective ohmic contact is difficult to be constructed between the metal-semiconductor interface due to the very thin HTM layer.²¹ The best device performance is achieved as the HTM concentration is 20 mg/mL. The worse cell performance at high HTM concentration (>20 mg/mL) could be ascribed to the elevated series resistance caused by the increased HTM layer thickness at higher concentration.⁹ At the range of 20-100 mg/mL, the higher *V_{oc}* at lower HTM concentration is mainly due to the declined dark current as the HTM film thickness decreased.²⁸ This results prove that suitable HTM layer thickness will facilitate the cell performance.

Time-resolved photoluminescence (PL) decay measurement has been conducted to understand the charge transfer (Figure S5) and the PL decay time (*τ*) are estimated by fitting the data with bi-exponential decay function.²⁹ Without HTM layer, the TiO₂/CH₃NH₃PbI₃ interface exhibits a long decay time of 102.18 ns. While a significantly reduced *τ* is observed for device with **TPBS** (34.2ns) and **TPBC** (11.4 ns), which indicates fast charge transfer at the CH₃NH₃PbI₃/HTM interface.²⁹ Besides, the charge transfer from perovskite to **TPBC** is faster than that of **TPBS**, which suggests that **TPBC** has better hole pumping capacity.⁹

In addition, the reproducibility of the cells' performance based on the new HTMs (**TPBS** and **TPBC**) are evaluated by testing photovoltaic parameters of ten cells. Related data are presented in Electronic Supporting Information. (Table S2[†]) The standard deviations of PCE for the cells with **TPBS** and **TPBC** is 0.36% and 0.26%, respectively. These results are indicating good reproducibility in our study.

Conclusions

In summary, two **TPB**-based HTMs (**TPBS** and **TPBC**) are successfully synthesized by a simple process with low cost. The HOMO and LUMO energy levels of these **TPB** derivatives are effectively tuned to match with perovskite by introducing electron-donating groups asymmetrically to the **TPB** core, which is demonstrated by optical and electrochemical studies. The perovskite solar cell based on **TPBC** as HTM without doping affords an impressive PCE of 13.10%, which is comparable to that obtained employing the well-known p-doping spiro-OMeTAD. This results provide compelling evidence for the first time that small-molecule HTMs with **TPB** core have great potential for the application in high efficient doping-free perovskite solar cell.

This work was supported by National High Technology

Research and Development Program of China (Grant No: 2012AA030307), National Natural Science Foundation of China (No. 21206110), Tianjin Science and Technology Support Program (13ZCZDZX00900), Beijing Science and Technology Committee (No. Z13110006013003) and Ministry of Science and Technology of China (973 projects, No. 2012CB932903).

Notes and references

^aDepartment of Applied Chemistry, School of Chemical Engineering and Technology, Tianjin University, Tianjin 300072, China. E-mail:

¹⁰ xiaoyin@tju.edu.cn

^bCollaborative Innovation Center of Chemical Science and Engineering (Tianjin), Tianjin 300072, China.

^cKey Laboratory for Renewable Energy, Chinese Academy of Sciences, Beijing 100190, China.

¹⁵ † Electronic Supplementary Information (ESI) available: [Experimental; Synthesis of HTMs; ¹H NMR, HRMS, elemental analysis. Additional figures of DSC, TG curve and CV, TOF measurement]. See DOI: 10.1039/b000000x/

- 1 J. Burschka, N. Pellet, S. -J. Moon, R. Humphry-Baker, P. Gao, M. K. Nazeeruddin, M. Grätzel, *Nature*, 2013, **499**, 316.
- 2 M. Liu, M. B. Johnston, H. J. Snaith, *Nature*, 2013, **501**, 3953.
- 3 D. Liu and T. L. Kelly, *Nat. Photonics*, 2014, **8**, 133.
- 4 H. Zhou, Q. Chen, G. Li, S. Luo, T.-B. Song, H.-S. Duan, Z. Hong, J. You, Y. Liu, and Y. Yang, *Science*, 2014, **345**, 542.
- 5 J. H. Heo, S. H. Im, J. H. Noh, T. N. Mandal, C.-S. Lim, J. A. Chang, Y. H. Lee, H.-J. Kim, A. Sarkar, M. K. Nazeeruddin, M. Grätzel, and S. I. Seok, *Nat. Photonics*, 2013, **7**, 486.
- 6 H. Li, K. Fu, A. Hagfeldt, M. Grätzel, S. G. Mhaisalkar and A. C. Grimsdale, *Angew. Chem. Int. Ed.*, 2014, **53**, 4085.
- 7 N. J. Jeon, J. Lee, J. H. Hoh, M. K. Nazeeruddin, M. Grätzel and S. I. Seok, *J. Am. Chem. Soc.*, 2013, **135**, 19087.
- 8 J. Wang, S. Wang, X. Li, L. Zhu, Q. Meng, Y. Xiao and D. Li, *Chem. Commun.*, 2014, **50**, 5829.
- 9 S. Lv, L. Han, J. Xiao, L. Zhu, J. Shi, H. Wei, Y. Xu, J. Dong, X. Xu, D. Li, S. Wang, Y. Luo, Q. Meng, and X. Li, *Chem. Commun.*, 2014, **50**, 6931.
- 10 T. Krishnamoorthy, F. Kunwu, P. P. Boix, H. Li, T. M. Koh, W. L. Leong, S. Powar, A. Grimsdale, M. Grätzel, N. Mathews and S. G. Mhaisalkar, *J. Mater. Chem. A*, 2014, **2**, 6305.
- 11 L. Zheng, Y.-H. Chung, Y. Ma, L. Zhang, L. Xiao, Z. Chen, S. Wang, B. Qu and Q. Gong, *Chem. Commun.*, DOI:10.1039/C4CC04680C.
- 12 J. Liu, Y. Wu, C. Qin, X. Yang, T. Yasuda, A. Islam, K. Zhang, W. Peng, W. Chen and L. Han, *Energy Environ. Sci.*, DOI: 10.1039/c4ee01589d.
- 13 P. Qin, S. Paek, M. I. Dar, N. Pellet, J. Ko, M. Grätzel, and M. K. Nazeeruddin, *J. Am. Chem. Soc.*, 2014, **136**, 8516.
- 14 K. Do, H. Choi, K. Lim, H. Jo, J. W. Cho, M. K. Nazeeruddin and J. Ko, *Chem. Commun.*, DOI: 10.1039/C4CC04550E.
- 15 A. K. Bansal and A. Penzkofer, *Appl. Phys. B*, 2008, **91**, 559-569.
- 16 Y. Song, C. Di, W. Xu, Y. Lin, D. Zhang and D. Zhu, *J. Mater. Chem.*, 2007, **17**, 4483.
- 17 G. Li, Y. F. Zhou, X. B. Cao, P. Bao, K. J. Jiang, Y. Lin and L. M. Yang, *Chem. Commun.*, 2009, **16**, 2201.
- 18 X. Ma, S. Wang, X. Li and Y. Xiao, *Org. Electron.*, 2014, **15**, 1876.
- 19 L. Yang, B. Xu, D. Bi, H. Tian, G. Boschloo, L. Sun, A. Hagfeldt and E. M. J. Johansson, *J. Am. Chem. Soc.*, 2013, **135**, 7378.
- 20 T. P. I. Saragi, T. F. Lieker and J. Salbeck, *Adv. Funct. Mater.*, 2006, **16**, 966.
- 21 Y. Xu, J. Shi, S. Lv, L. Zhu, J. Dong, H. Wu, Y. Xiao, Y. Luo, S. Wang, D. Li, X. Li and Q. Meng, *ACS Appl. Mater. Interfaces*, 2014, **6**, 5651.
- 22 Y. Song, X. Li, S. Wang and Y. Xiao, *2012 AIChE Annual Meeting*, ISBN:978-0-8169-1073-1.
- 23 Y. Wu and W. Zhu, *Chem. Soc. Rev.*, 2013, **42**, 2039.
- 24 D. Poplavskyy and J. Nelson, *J. Appl. Phys.*, 2002, **93**, 341.

- 25 J. A. Christians, R. C. M. Fung and P. V. Kamat, *J. Am. Chem. Soc.*, 2014, **136**, 758.
- 26 H.-S. Kim, J.-W. Lee, N. Yantara, P. P. Boix, S. A. Kulkarni, S. Mhaisalkar, M. Grätzel and N.-G. Park, *Nano Lett.*, 2013, **13**, 2412.
- 27 H.-S. Kim, I. Mora-Seró, V. Gonzalez-Pedro, F. Fabregat-Santiago, E. J. Juarez-Perez, N.-G. Park and J. Bisquert, *Nat. Commun.*, 2013, **4**, 2242.
- 28 H.-S. Kim, C.-R. Lee, J.-H. Im, K.-B. Lee, T. Moehl, A. Marchioro, S.-J. Moon, R. Humphry-Baker, J.-H. Yum, J. E. Moser, M. Grätzel and N.-G. Park, *Sci Rep*, 2012, **2**, 591.
- 29 J. You, Z. Hong, Y. Yang, Q. Chen, M. Cai, T.-B. Song, C.-C. Chen, S. Lu, Y. Liu, H. Zhou and Y. Yang, *ACS nano*, 2014, **8**, 1674.

Graphical Abstract

Two *N,N,N',N'*-tetraphenyl-benzidine-based HTMs were synthesized. Their energy levels were tuned to match with perovskite by introducing electron-donating groups. The TPBC based doping-free perovskite solar cell afforded an impressive PCE of 13.10% under AM 1.5G ($100\text{mW}\cdot\text{cm}^{-2}$), which is the first demonstration for effective device with TPB-based doping-free HTMs.

